NeuroImage 124 (2016) 693–703

Contents lists available at ScienceDirect

NeuroImage

journal homepage: www.elsevier.com/locate/ynimg

Decoupled temporal variability and signal synchronization of spontaneous brain activity in loss of consciousness: An fMRI study in anesthesia

Zirui Huang [a,b,*,1], Jun Zhang [a,**,1], Jinsong Wu [c,1], Pengmin Qin [b], Xuehai Wu [c], Zhiyao Wang [a], Rui Dai [d,e,f], Yuan Li [g], Weimin Liang [a], Ying Mao [c], Zhong Yang [g], Jianfeng Zhang [d,e], Annemarie Wolff [b], Georg Northoff [b,d,e]

[a] Department of Anesthesiology, Huashan Hospital, Fudan University, Shanghai 200040, PR China
[b] Institute of Mental Health Research, University of Ottawa, Ottawa, ON K1Z 7K4, Canada
[c] Department of Neurosurgery, Huashan Hospital, Fudan University, Shanghai 200040, PR China
[d] Center for Cognition and Brain Disorders, Hangzhou Normal University, Hangzhou 310003, PR China
[e] Zhejiang Key Laboratory for Research in Assessment of Cognitive Impairments, Hangzhou Normal University, Hangzhou 310015, PR China
[f] School of Life Science, South China Normal University, Guangzhou 510613, PR China
[g] Department of Radiology, Huashan Hospital, Fudan University, Shanghai 200040, PR China

ARTICLE INFO

Article history:
Received 18 March 2015
Accepted 27 August 2015
Available online 4 September 2015

Keywords:
Anesthesia
fMRI
Resting-state
Consciousness
Temporal variability
Signal synchronization

ABSTRACT

Two aspects of the low frequency fluctuations of spontaneous brain activity have been proposed which reflect the complex and dynamic features of resting-state activity, namely temporal variability and signal synchronization. The relationship between them, especially its role in consciousness, nevertheless remains unclear. Our study examined the temporal variability and signal synchronization of spontaneous brain activity, as well as their relationship during loss of consciousness. We applied an intra-subject design of resting-state functional magnetic resonance imaging (rs-fMRI) in two conditions: during wakefulness, and under anesthesia with clinical unconsciousness. In addition, an independent group of patients with disorders of consciousness (DOC) was included in order to test the reliability of our findings. We observed a global reduction in the temporal variability, local and distant brain signal synchronization for subjects during anesthesia. Importantly, we found a link between temporal variability and both local and distant signal synchronizations during wakefulness: the higher the degree of temporal variability, the higher its intra-regional homogeneity and inter-regional functional connectivity. In contrast, this link was broken down under anesthesia, implying a decoupling between temporal variability and signal synchronization; this decoupling was reproduced in patients with DOC. Our results suggest that there exist some as yet unclear physiological mechanisms of consciousness which "couple" the two mathematically independent measures, temporal variability and signal synchronization of spontaneous brain activity. Our findings not only extend our current knowledge of the neural correlates of anesthetic-induced unconsciousness, but have implications for both computational neural modeling and clinical practice, such as in the diagnosis of loss of consciousness in patients with DOC.

Introduction

Recent studies of resting-state brain activity have contributed to our understanding of organization and integration in large-scale brain networks. From these significant findings, two aspects of the low frequency fluctuations (Biswal et al., 1995; Fox and Raichle, 2007; Zhang and Raichle, 2010) of spontaneous brain activity were suggested. These features reflect the complex and dynamic features of resting-state activity, temporal variability and signal synchronization/correlation specifically.

In the first instance, there is evidence suggesting that temporal variability is a central measure of large-scale brain activities (Deco et al., 2009, 2011; Faisal et al., 2008; Garrett et al., 2010, 2011, 2013a,b; He, 2011; McIntosh et al., 2010; Shew et al., 2009, 2011; Vakorin et al., 2011). Higher temporal variability in the resting-state has been observed in regions that constitute the default-mode, as well as in the thalamocortical networks (Zang et al., 2007). Furthermore, higher temporal variability reflects a greater dynamic range of possible responses to incoming stimuli. This is beneficial to the adaptability and efficiency

* Correspondence to: Z. Huang, University of Ottawa, Institute of Mental Health Research, Room 6440, 1145 Carling Avenue, Ottawa, ON K1Z 7K4, Canada. Fax: +1 613 798 2982.
** Correspondence to: J. Zhang, Department of Anesthesiology, Huashan Hospital, Fudan University, 12#, Wulumuqi Zhong Road, Shanghai 200040, PR China. Fax: +86 21 52887690.
E-mail addresses: Dr.Zirui.Huang@gmail.com (Z. Huang), snapzhang@aliyun.com (J. Zhang).
[1] Authors contributed equally to this work.

http://dx.doi.org/10.1016/j.neuroimage.2015.08.062
1053-8119/

of neural systems as it permits a greater range of response to a greater range of stimuli (Garrett et al., 2013c). In contrast, when variability is lacking, there is little capacity for the brain to explore its state space. This increases the possibility of the system to remain rigidly in a single state (Deco et al., 2009; Deco and Jirsa, 2012), making state-to-state transitions more difficult, either spontaneously or when required (Garrett et al., 2013c).

In the second feature, brain signal synchronization describes the degree of coordination of brain activity within-regional homogeneity (Zang et al., 2004; Zuo et al., 2010, 2013) and between-functional connectivity (Biswal et al., 1995; Cordes et al., 2000; Greicius et al., 2003, 2004) regions. Unfortunately, these signal synchronization metrics scale away temporal variability in their calculation. Nevertheless, the examination of potential links between temporal variability and signal synchronization is inherently interesting. Using resting-state functional magnetic resonance imaging (rs-fMRI) and biologically informed computational modeling (Deco et al., 2013; Wong and Wang, 2006), Yang et al. (2014) demonstrated how alterations in local (recurrent self-coupling) and distant (long-range coupling) signal synchronization impact temporal variability in the context of schizophrenia — another extreme example of a conscious state. Their modeling results revealed that the temporal variability increased as a function of increasing local and distant signal synchronization. It was also suggested that the observed increase in temporal variability in schizophrenia may arise from increased neural coupling at both local and long-range scales, leading to a cortical network that operates closer to the edge of instability than in awake healthy subjects (Yang et al., 2014). Importantly, this study gave us an indication that the relationship between the temporal variability and signal synchronization may be conscious relevant. Evidence, however, regarding the variety of the states of consciousness, is still lacking.

Other studies in altered states of consciousness, such as in anesthesia and disorders of consciousness (DOC), have reported abnormal temporal variability (Huang et al., 2014a,b) and decreased signal synchronization in the frontoparietal and thalamocortical networks (Boveroux et al., 2010; Demertzi et al., 2014; Kotchoubey et al., 2013; Mashour, 2006; Palanca et al., 2015; Schrouff et al., 2011; Vanhaudenhuyse et al., 2010; White and Alkire, 2003). However, the exact relationship between the temporal variability and signal synchronization, especially its functional role in consciousness, was yet to be attempted.

With that in mind, the aim of our study was to examine said relationship: is there a connection between temporal variability and signal synchronization during wakefulness, and, if so, does this change during loss of consciousness under anesthesia? To address this question, we first applied an intra-subject design of rs-fMRI for a group of subjects during two conditions: a) wakefulness, and b) under anesthesia with clinical unconsciousness. Next, in order to examine if the result of anesthesia is reproducible in other altered states of consciousness, which can in turn further rule out potential drug effects of anesthesia, we included an independent group of patients with disorders of consciousness (DOC), as well as a healthy control (HC) group. Three resting-state measures were including in our analysis: (1) the standard deviation (SD) of BOLD signal across time (Garrett et al., 2010, 2011) was utilized for the examination of the temporal variability of spontaneous brain activity (Huang et al., 2014a,b); (2) the regional homogeneity (ReHo) was employed to measure local signal synchronization (Zang et al., 2004; Zuo et al., 2010, 2013); and (3) the degree of centrality (DC) was determined in order to examine distant signal synchronization (Buckner et al., 2009; Di Martino et al., 2013; Zuo et al., 2012). Finally, using a region-based correlation approach (He et al., 2010; He, 2011, 2013), we correlated these measures for both the awake and anesthesia conditions respectively, and examined the differences of these correlations between the two states. An identical analysis pipeline was applied to the DOC and HC groups.

Material and methods

Subjects during wakefulness and under anesthesia

Twelve subjects undergoing an elective trans-sphenoidal approach for resection of a pituitary microadenoma were included in this study (5 female; 26–62 years). The pituitary microadenomas were diagnosed by their size (<10 mm in diameter without sella expansion) based on radiological examinations and plasma endocrinal indicators. These patients were ASA (American Society of Anesthesiologists) physical status I or II grade. The subjects had no history of craniotomy, cerebral neuropathy, or vital organ dysfunction. This study was approved by the Ethics Committee of Huashan Hospital, Fudan University. Written informed consent was obtained from all subjects.

Protocol of anesthesia

The subjects were randomly divided into two groups, those receiving intravenous propofol anesthesia (n = 6) and those receiving inspiratory sevoflurane anesthesia (n = 6). Propofol, one of the intravenous anesthetics, selectively modulates $GABA_A$ receptors by enhancing the gating of the receptors by GABA (Hales and Lambert, 1991; Tomlin et al., 1998) which in turn reduces neuronal excitability (Franks, 2006). Sevoflurane, one of the inhaled anesthetics, enhances $GABA_A$ receptor function (Krasowski and Harrison, 1999) by increasing channel opening, hereby enhancing inhibition at both synaptic and extrasynaptic receptors (Hemmings et al., 2005). For the group receiving propofol, a target-controlled infusion (TCI) was used to set plasma concentration of propofol at 3.0–5.0 μg/ml, followed by remifentanil (1.0 μg/kg) and succinylcholine (1.5 mg/kg) to facilitate endotracheal intubation. The TCI propofol was maintained at a stable effect-site concentration (4.0 μg/ml) to reliably induce an unconscious state (Xu et al., 2009). For the group receiving sevoflurane, anesthesia induction was completed with 8% sevoflurane in 100% oxygen, adjusting fresh gas flow to 6 l/min, combined with remifentanil (1.0 μg/kg) and succinylcholine (1.0 mg/kg), and maintained with 2.6% (1.3 MAC) ETsevo in 100% oxygen, fresh gas flow at 2.0 l/min. The concentration of sevoflurane used in our study also fulfilled the requirement to maintain loss of consciousness in patients classified as ASA physical status I or II (Katoh and Ikeda, 1998). Considering the quick elimination of the analgesic remifentanil and depolarized neuromuscular relaxant succinylcholine from plasma, the effects of drugs on the brain during anesthesia can be attributed solely to propofol or sevoflurane in each respective group.

After the induction of anesthesia, the subjects were ventilated with intermittent positive pressure ventilation, setting the tidal volume at 8–10 ml/kg, the respiratory rate at 10–12 beats per minute, and maintaining $PetCO_2$ (end tidal partial pressure of CO_2) at 35–40 mm Hg. All subjects fulfilled the criteria of deep sedation; neither response to verbal command ("strongly squeeze my hand!"), nor response to prodding or shaking was observed during anesthesia, corresponding to Ramsay 5–6 (Boveroux et al., 2010) and an OAA/S score of 1 (Chernik et al., 1990; Liu et al., 2009; Zhang et al., 2009; Quan et al., 2013). In addition, no subject reported explicit memory in the post-operative follow-up. Therefore, all subjects were considered unconscious during anesthesia.

Patients with disorders of consciousness (DOC) and healthy controls

To verify the results of wakefulness vs. anesthesia, we included 12 DOC patients and 12 healthy controls (HC). Of note, the resting-state fMRI data of these DOC patients were selected from a data-base with a large sample of patients (n = 96) from Huashan hospital and its affiliated rehabilitation centers. Specifically, we first excluded patients with obvious brain lesions or distortions, thus making the results comparable with subjects under anesthesia as structural changes of the brain may confound the spatial transformation (into standard space) during data preprocessing. This screened 12 patients with well-preserved brains,

and the sample size also matched our anesthesia group (n = 12). The DOC patients were assessed using the Coma Recovery Scale — Revised (CRS-R) (Giacino et al., 2004) on the day of fMRI scanning (see Supplementary Table 1 for the clinical information). Eight patients were diagnosed as unresponsive wakefulness syndrome/vegetative state (UWS/VS), and four were diagnosed as minimally conscious state (MCS). Due to the limited number of patients, UWS/VS and MCS were collapsed into one group constituting our DOC group. In addition, 12 age/gender matched healthy controls were selected from the same data-base of 52 healthy subjects. For the healthy controls, none had a history of neurological or psychiatric disorders, nor were they taking any kind of medication. Informed written consent was obtained from the patients' legal representatives, and from the healthy participants. The study was also approved by the Ethics Committee of Shanghai Huashan Hospital, Fudan University.

fMRI data acquisition

For subjects during wakefulness and under anesthesia, an intraoperative Siemens 3 T scanner (Siemens MAGNETOM, Germany) with a standard head coil was used to acquire gradient-echo EPI images of the whole brain (25 slices, TR/TE = 2000/30 ms, slice thickness = 6 mm, field of view (FOV) = 192 mm, flip angle = 90°, image matrix: 64 × 64). In addition, high-resolution anatomical images were acquired. Two 8 m rs-fMRI volumes were acquired during wakefulness and under anesthesia. During the wakefulness scan, the subject's head was fixed in the scan frame to limit its movement. The subjects were instructed to wear earplugs, take a comfortable supine position, to relax with their eyes closed, and not to concentrate on anything in particular. Eye-tracking during fMRI was not available, but off-line post-scan recordings ensured that subjects did comply with this instruction. The subjects were anesthetized after the wakefulness scan and given full hydration with hydroxyethyl starch to avoid hypotension. Fifteen minutes after stabilization of anesthetic levels and hemodynamics, the anesthetized state scan was performed.

For the DOC patients and healthy controls, all MR images were acquired on another Siemens 3 T scanner. EPI images were also acquired for the whole brain (33 slices, TR/TE = 2000/35 ms, slice thickness = 4 mm, field of view (FOV) = 256 mm, flip angle = 90°, image matrix: 64 × 64). Two hundred EPI volumes as well as high-resolution anatomical images were acquired. All subjects were instructed by the same researcher to take a comfortable supine position, to relax, close their eyes, and to not concentrate on anything in particular during the scanning. All participants wore earplugs to minimize the noise of the scanner.

fMRI data preprocessing

Preprocessing steps were implemented in AFNI (Cox, 1996). After discarding the first two volumes, the functional images from each scan were aligned (head motion correction), slice timing corrected, temporally standardized, resampled to $3 \times 3 \times 3$ mm^3, spatially smoothed (6-mm full width at half maximum Gaussian blur), transformed into Talaraich space (Talairach and Tournoux, 1988), and linear trends were removed. The data was then filtered with a band-pass filter preserving signals between 0.01 and 0.08 Hz, which is thought to reflect fluctuations of spontaneous brain activity (Fox and Raichle, 2007; Zhang and Raichle, 2010). The estimated six parameters of head motion and mean time series from the white matter (WM) and cerebrospinal fluid (CSF) were regressed out. To minimize partial voluming with gray matter, the WM and CSF masks were eroded by one voxel (Chai et al., 2012).

The issue of motion artifacts was addressed rigorously as minor group differences in motion have been shown to artificially create between-groups differences (Power et al., 2012; van Dijk et al., 2012). We first calculated the indices of the amount of motion (shift and rotation) for each subject (Zang et al., 2007). No difference (wakefulness vs. anesthesia) was observed for either shift or rotation by paired sample t-tests (Supplementary Fig. 1). In addition, the number of 'outliers' for the data at each time point was calculated to tag the outliers of global signal intensity and motion by AFNI program 3dToutcount. The time points with head motion greater than 0.3 mm per TR and/or outliers comprising more than 10% were excluded from the following analysis. Furthermore, to exclude the potential confound of head motion, we performed standard GLM analyses, including head motion indices as covariates, for all the following group-level analysis. An identical analysis pipeline was applied to the DOC and HC groups. One DOC patient (No. 6) was excluded from the further analyses due to excessive and large movements during scanning (shift > 3 mm, rotation > 3°; in each direction).

Standard deviation (SD) of BOLD signal — temporal variability

The standard deviation (SD) of blood oxygenation level-dependent (BOLD) signal (Garrett et al., 2010, 2011) describes the temporal variability of fluctuations in BOLD-fMRI signals across time within a particular region. The SD across the time series for each voxel was calculated to yield an SD map for each subject. In addition, we performed a control analysis using a normalization procedure (Zuo et al., 2010). Specifically, subject-level voxel-wise SD maps were standardized into subject-level Z-score maps (SD-Z) per brain volume by subtracting the mean voxel-wise SD obtained for the entire brain (global mean of SD) and then dividing by the standard deviation across voxels (Zuo et al., 2010). This normalization procedure (Z-transform across voxels) changed the absolute values of SD; post-normalization they conformed to a Z-distribution without changing the spatial pattern of value distribution across voxels.

Regional homogeneity (ReHo) — local synchronization

Regional homogeneity (ReHo) measures intra-regional (local) synchronization which is the coordination of activity between voxels within a region (Zang et al., 2004). Specifically, for each voxel, Kendall's coefficient of concordance (KCC) was calculated between the BOLD time series for the specified voxel and those of its 26 nearest neighbors (Zang et al., 2004; Zuo et al., 2013)

$$W = \frac{\sum (R_i)^2 - n(\overline{R})^2}{\frac{1}{12}K^2(n^3 - n)}$$

where W is the KCC among given voxels, ranged from 0 to 1; R_i is the sum rank of the ith time point; where $\overline{R} = ((n+1)/K)/2$ is the mean of the R_i's; K is the number of time series within a measured cluster (here, $K = 27$; one given voxel plus the number of its neighbors); and n is the number of ranks (here $n = 238$, according to 238 volumes in the data). ReHo analysis was performed for each subject by AFNI program: *3dReHo*, giving a voxel-wise ReHo map. As spatial smoothing could artificially enhance ReHo intensity and reduce its reliability (Zuo et al., 2013), we calculated ReHo based on non-smoothed BOLD time series. After this, spatial smoothing was performed with a 6-mm full-width at half-maximum (FWHM) Gaussian kernel for the ReHo map. In addition, similar to the above calculation of SD-Z, the individual ReHo map was standardized into subject-level Z-score maps (ReHo-Z) by subtracting the mean voxel-wise ReHo obtained for the entire brain (global mean of ReHo) then dividing by the standard deviation across voxels (Zuo et al., 2010, 2013).

Degree of centrality (DC) — distant synchronization

In graph theory, a complex system is modeled as a "graph", which is defined as a set of "nodes" linked by "edges". For a binary graph, degree of centrality (DC) is the number of edges connecting to a node. For a weighted graph, DC is defined as the sum of weights from edges

connecting to a node, which is also sometimes referred to as the node strength (Zuo et al., 2012). The DC analysis was performed for each subject by AFNI program *3dTcorrMap*. Specifically, voxel-based graphs were generated for each participant. Each voxel constitutes a node in the graph and each significant functional connection (Pearson correlation) between any pair of voxels is an edge. A voxel-based graph is thus a mathematical representation of the functional network consisting of nodes or voxels and their edges or connections (Buckner et al., 2009; Di Martino et al., 2013; Zuo et al., 2012). To obtain each participant's graph, the correlation between the time series of each voxel with every other voxel in the individual whole brain mask was computed. A binary, undirected adjacency matrix was then obtained by thresholding each correlation at $r > 0.3$. Based on the graph, DC was calculated at the individual level (Zuo et al., 2012). We computed DC by counting the number of functional connections (positive correlations) between each voxel and all other voxels. In addition, normalized DC (DC-Z) indices were calculated by transforming DC to Z-scores based on the global mean of DC and standard deviation across voxels in the brain (Buckner et al., 2009; Di Martino et al., 2013; Zuo et al., 2012).

To examine if our results are robust regarding the choice of threshold, we applied a range of thresholds ($0.1 \le r \le 0.8$, 0.1 increments) to binarize the correlation matrix. The DC indices for each threshold was calculated and then divided by the expected number of such suprathreshold voxels that would occur from white noise time series, using the option of "*−VarThreshN*" in *3dTcorrMap*. Both DC and DC-Z were obtained for each threshold and each subject.

Group analysis of whole brain SD, ReHo and DC

The non-normalized and normalized SD, ReHo, and DC maps were tested in paired t-tests, respectively, to examine the differences between wakefulness ($n = 12$) and under anesthesia ($n = 12$). Three potential confounds were used as covariates: 1) head motion indices, 2) type of anesthetic agent (propofol and sevoflurane), and 3) age. Specifically, we performed stand GLM analyses without covariate, with single covariate, and with all three covariates (main results) to examine the consistency of our results. Unless otherwise stated, all resulting t-maps were thresholded at a corrected p-value of <0.05. That is, the multiple-comparison error was corrected using Monte Carlo simulation as implemented in AFNI program AlphaSim, yielding a family-wise error rate (FWER) at $p < 0.05$ with a minimal cluster size of 97 voxels. The smoothness used in the AlphaSim was the average smoothness across subjects. To test whether group differences (wakefulness vs. anesthesia) are due to the effects of the physiological impacts of the anesthetic agent used, or if these are actually markers of consciousness, we performed a two-way ANOVA to examine the potential interaction effect between conscious state (awake and anesthetized) and type of anesthetic agent (propofol and sevoflurane).

Defining nodes of intrinsic connectivity networks

We used the 8 min resting state of each subject during wakefulness to analyze resting-state functional connectivity (rs-fc). We thereby defined the default mode network (DMN) (Raichle et al., 2001) as well as three other large-scale networks, namely the salience network (SN) (Eckert et al., 2009; Sadaghiani et al., 2010; Seeley et al., 2007), executive-control network (ECN) (Fox et al., 2005; Seeley et al., 2007) and sensorimotor network (SMN) (de Pasquale et al., 2012; Heine et al., 2012). Seed regions for calculating rs-fc networks were voxels in a sphere of 6 mm radius centered on stereotactic coordinates reported by other laboratories: (1) posterior cingulate cortex (PCC)/precuneus (−4, −52, 22) for the DMN (Laird et al., 2009); (2) right caudal anterior cingulate cortex (4, 16, 33) for the SN (Seeley et al., 2007); (3) left dorsolateral prefrontal cortex (−32, 41, 13) for the ECN (Seeley et al., 2007); and (4) left central sulcus (−36, −24, 49) for the SMN (Pasquale et al., 2012). Next, for each of the four seed regions, voxel-wise rs-fc maps to a given seed were computed as maps of temporal correlation coefficients between BOLD time course in each voxel and BOLD time course averaged across voxels in the seed region. Contrast images were created for each subject then transformed by Fisher's Z transform for second-level one-sample t-tests. The group rs-fc maps of the DMN, SN, ECN and SMN were defined as the non-overlapping voxels from each of the other maps at threshold $p < 0.005$, uncorrected, cluster extent > 100 voxels. Nodes of intrinsic connectivity in the subsequent analysis were defined as voxels in a sphere of 6 mm radius centered on each cluster of the networks. In order to balance the number of nodes across networks, only the largest 6 clusters – sorted by cluster size – were included, yielding a total of 24 nodes across the 4 networks.

Node-based correlation analysis

For each node, the values of SD, ReHo and DC were extracted from each subject and averaged across subjects for both wakefulness and under anesthesia, respectively. To establish the association between temporal variability (SD), local (ReHo), and distant (DC) signal synchronization, Pearson correlation analyses (95% confidence interval based on 1000 bootstrap samples) were performed on each pair of measures, namely SD ∝ ReHo, SD ∝ DC and ReHo ∝ DC, across the 24 nodes for both wakefulness and under anesthesia, respectively. This region-based approach could also counter between-subject measurement noise (He et al., 2010; He, 2011, 2013). Next, the correlation coefficients for each pair of measures were compared between wakefulness and under anesthesia. This analysis pipeline was also applied to the normalized measures, SD-Z ∝ ReHo-Z, SD-Z ∝ DC-Z and ReHo-Z ∞ DC-Z.

To confirm that the above node-based correlation analysis at the group level was not due to individual noise, we performed group comparisons based on individual correlation coefficients. Specifically, the correlation coefficients of SD ∝ ReHo, SD ∝ DC and ReHo ∝ DC, as well as normalized pairs, were first calculated for each subject, and then transformed into Fisher's Z scores. Next, paired sample t-tests were performed between wakefulness and under anesthesia.

In light of the fact that the correlation between SD and DC may be confounded by local synchronization (ReHo), we further performed a partial Pearson correlation (95% confidence interval based on 1000 bootstrap samples) between SD and DC by including ReHo as a covariate. The same procedure was applied to SD-Z ∝ DC-Z using ReHo-Z as a covariate.

To confirm that our findings did not dependent upon the definition of nodes, we repeated our calculation, as described above, by using another nodes' template which had previously been well-defined (He et al., 2010; He, 2011, 2013). The template contains 31 ROIs including attention, default-mode, motor, saliency, and visual networks, as well as the hippocampus, thalamus and cerebellum (see Table 1 in He, 2011). One node in the medial prefrontal cortex was excluded due to relatively higher signal dropout (Preston et al., 2004).

Finally, to examine if the result of anesthesia is reproducible in other altered states of consciousness, and to rule out potential drug effects of the anesthesia, we applied the same node-based correlation analysis (30 ROIs defined as above) in an independent group of DOC patients and a healthy control (HC) group.

Results

Whole brain SD, ReHo and DC (wakefulness vs. unconsciousness)

The comparison between wakefulness and unconsciousness (under anesthesia) for the SD, ReHo and DC showed a remarkable reduction across wide-spread cortical regions during unconsciousness (Fig. 1A; see Supplementary Fig. 2 for normalized measures, i.e., SD-Z, ReHo-Z and DC-Z). This was confirmed by comparing the global mean (wakefulness vs. unconsciousness) of SD ($t_{(11)} = 4.51$, $p = 0.001$), ReHo ($t_{(11)} = 4.91$, $p = 0.000$) and DC ($t_{(11)} = 4.07$, $p = 0.002$) (Fig. 1B). No

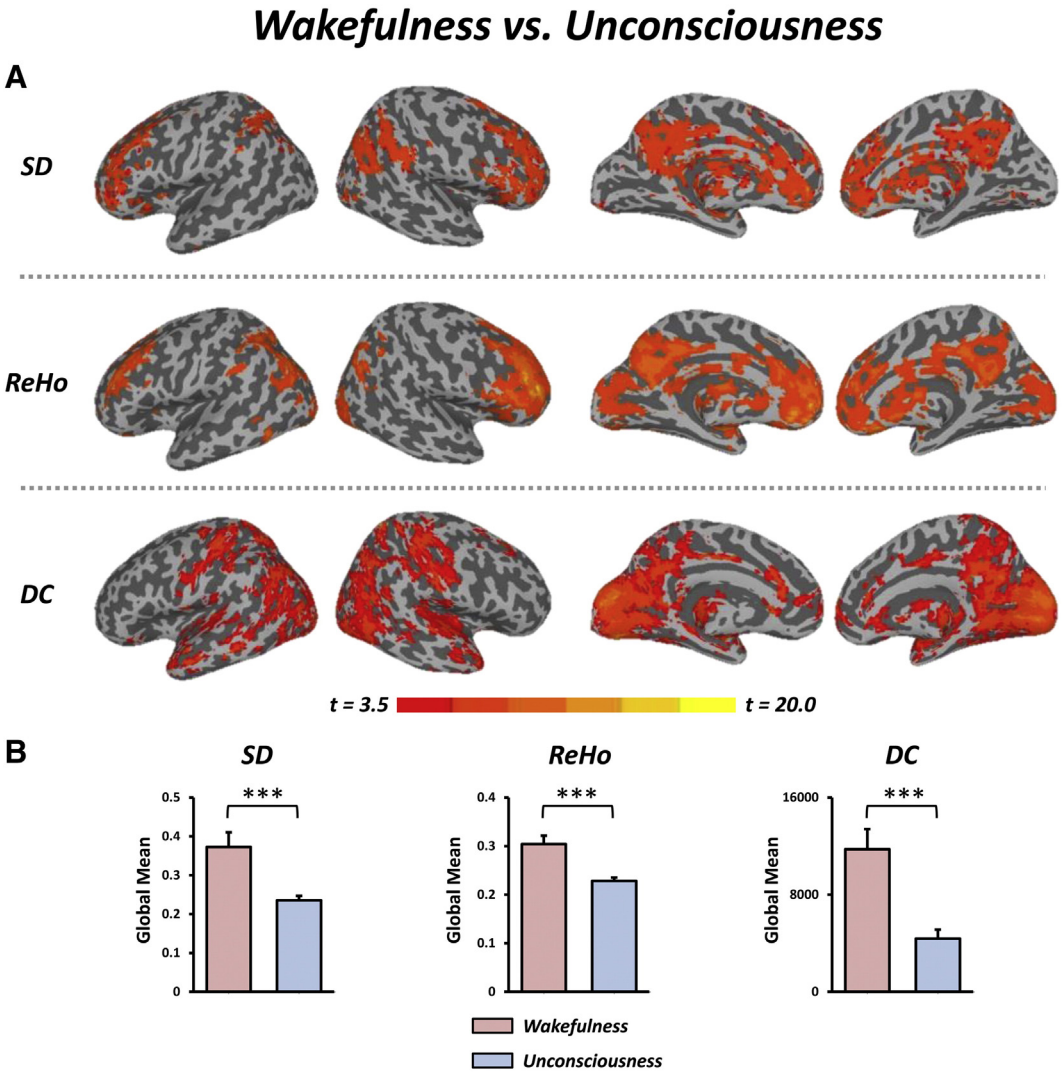

Fig. 1. Temporal variability, local and distant signal synchronization (wakefulness vs. unconsciousness). A. Group comparison of SD, ReHo and DC. All t-maps were thresholded at corrected $p < 0.05$. The color bar shows voxel-wise t-values. B. Comparisons of global mean (across voxels of the whole brain) for SD, ReHo and DC. $^{***}p < 0.005$. SD: standard deviation of BOLD signal describing the temporal variance of brain activity; ReHo: regional homogeneity indicating local signal synchronization; and DC: degree of centrality indicating distant signal synchronization.

interaction effect between conscious state (awake and anesthetized) and type of anesthetic agent (propofol and sevoflurane) was observed for any measure, either with or without normalization, suggesting that the above observed differences are consciousness relevant rather than the physiological impacts of the anesthetic agent used. In the following results, the two groups were pooled into one in order to enlarge the sample size. We further confirmed our observation using type of anesthetic agent, head motion and age as covariates in standard GLM analyses. Again, consistent results were seen by comparing the results without covariate, with single covariate, and with all covariates (see Supplementary Figs. 3, 4, and 5).

Node-based correlations between SD, ReHo and DC

Twenty-four nodes were defined from four distinct networks: the default mode (DMN), the salience (SN), executive-control (ECN) and sensorimotor networks (SMN), identified by seed-based functional connectivity analysis (Table 1; Fig. 2A). The networks that we obtained here are in agreement with previous studies (Eckert et al., 2009; Fox et al., 2005; Greicius et al., 2003; Heine et al., 2012; Laird et al., 2009; De Pasquale et al., 2012; Raichle et al., 2001; Sadaghiani et al., 2009; Seeley et al., 2007).

The relationship between temporal variability (SD), local (ReHo), and distant (DC) signal synchronization was established by correlating each pair of measures for both wakefulness and unconsciousness, respectively. During wakefulness, significant positive correlations were observed for SD ∝ ReHo ($r = 0.758$, $p < 0.001$), SD ∝ DC ($r = 0.778$, $p < 0.001$) and ReHo ∝ DC ($r = 0.731$, $p < 0.001$). In contrast, no significant correlation was found in either SD ∝ ReHo ($r = 0.287$, $p = 0.174$) or SD ∝ DC ($r = 0.297$, $p = 0.158$), whereas ReHo ∝ DC remained significant ($r = 0.841$, $p < 0.001$) during unconsciousness (Fig. 2B). Furthermore, we observed significant differences between wakefulness and unconsciousness in both SD ∝ ReHo ($Z = 3.19$, $p = 0.0014$) and SD ∝ DC ($Z = 3.36$, $p = 0.0008$), while no difference was seen in ReHo ∝ DC ($Z = -1.35$, $p = 0.177$). In a next step, we confirmed that our node-based correlation analysis at the group level is not due to individual noise, as the group difference still holds based on individual correlation coefficients (Fig. 2C). Additionally, one might argue that the significant correlation between SD and DC during wakefulness could be confounded by regional synchronization (ReHo). We confirmed

Table 1
Nodes of four distinct intrinsic connectivity networks identified with seed-based functional connectivity analysis.

Anatomical region	Abbreviation	BA	x	y	z
Default mode network (DMN)					
Posterior cingulate cortex	PCC	31	0	−54	23
Medial prefrontal cortex	MPFC	9	0	43	25
L middle temporal gyrus	L-MTG	22	−54	−12	−6
L angular gyrus	L-AG	39	−43	−63	30
R angular gyrus	R-AG	39	48	−59	28
R middle temporal gyrus	R-MTG	21	58	−17	−6
Salience network (SN)					
Caudal anterior cingulate cortex	cACC	24	1	6	37
R thalamus	R-Tha	–	10	−13	12
L insula	L-Ins	13	−32	15	8
R insula	R-Ins	13	33	16	4
R superior frontal gyrus	R-SFG	9	30	40	31
L superior frontal gyrus	L-SFG	9	−30	42	32
Executive control network (ECN)					
L dorsolateral prefrontal cortex	L-DLPFC	9	−38	22	28
L inferior parietal lobule	L-IPL	40	−40	−52	44
R middle frontal gyrus	R-MFG	6	39	7	41
R dorsolateral prefrontal cortex	R-DLPFC	10	35	41	12
R culmen	R-Cul	–	30	−63	−26
L medial frontal gyrus	L-MFG	6	2	−22	51
Sensorimotor network (SMN)					
L postcentral gyrus	L-PostC	2	−39	−24	44
R precentral gyrus	R-PreC	6	49	−15	34
R cuneus	R-Cun	18	2	−85	20
R superior parietal lobule	R-SPL	5	23	−42	59
R declive	R-Dec	–	17	−54	−12
R precuneus	R-PreCu	7	26	−77	31

BA, Brodmann area; R, right; L, left. x, y, z coordinates are provided in Talairach space.

that the correlation of SD ∝ DC remained significant ($r = 0.504$, $p = 0.014$) by including ReHo as a covariate. Similar results were seen for the normalized measures (Supplementary Fig. 6).

Several other potential confounds were addressed in order to confirm our results. First, as graph theoretical results (DC) may be dependent on the threshold used, we applied a range of thresholds ($0.1 \le r \le 0.8$, 0.1 increments) to binarize the correlation matrix. We confirmed that our results were robust to the choice of threshold in terms of the relationships between SD and DC, as well as ReHo and DC. That is, the group differences (wakefulness vs. unconsciousness) in SD ∝ DC were significant across all thresholds applied ($p < 0.005$), while no significant difference was seen in ReHo ∝ DC for any threshold (Fig. 3A). Similar results were observed for the normalized measures (Supplementary Fig. 7). Second, to examine whether our results had any bias on the nodes' definition, we repeated our calculation using another nodes' template (He et al., 2010; He, 2011, 2013). As expected, we found similar results (Fig. 3B), indicating that our analysis was not substantially affected by nodes selection.

Third, to examine if the result of anesthesia is reproducible and to rule out potential drug effects of the anesthesia, we compared the correlations between SD, ReHo and DC in both DOC and HC groups. As expected, significant positive correlations were observed for the HC in SD ∝ ReHo ($r = 0.766$, $p < 0.001$), SD ∝ DC ($r = 0.413$, $p = 0.023$) and ReHo ∝ DC ($r = 0.425$, $p = 0.019$). In contrast, no significant correlation was found for the DOC in either SD ∝ ReHo ($r = -0.349$, $p = 0.058$) or SD ∝ DC ($r = -0.045$, $p = 0.812$), whereas ReHo ∝ DC remained significant ($r = 0.538$, $p = 0.002$) (Fig. 4A). We also confirmed the group difference using individual correlation coefficients (Fig. 4B). Again, similar results were observed for the normalized measures (Supplementary Fig. 8). In addition, the unconscious patients (under anesthesia) and DOC were compared by ANCOVA with scanner type (1 for the first scanner data, and 2 for the second) as a covariate. No significant difference between the two groups was observed in either SD ∝ ReHo ($p = 0.136$) or SD ∝ DC ($p = 0.833$) by posthoc t-tests (Supplementary Fig. 9).

Discussion

We reported various measures of resting-state activity – temporal variability measured by the standard deviation of BOLD signal (SD), local and distant brain signal synchronization measured by regional homogeneity (ReHo), and degree of centrality (DC) respectively – in anesthesia. We observed a global reduction in SD, ReHo and DC for subjects under anesthesia. Importantly, we found a link between SD, ReHo and DC during wakefulness: the higher the degree of temporal variability, the higher its intra-regional homogeneity and inter-regional functional connectivity. In contrast, this link was broken down in anesthesia, implying a decoupling between temporal variability and signal synchronization; this decoupling was reproduced in patients with DOC (see Fig. 5 for a summary of our results). Our results imply that there appears to be some as yet unclear physiological mechanisms of consciousness which "couple" the two mathematically independent measures, temporal variability and signal synchronization of spontaneous brain activity. Our findings not only extend our current knowledge of the neural correlates of anesthetic-induced unconsciousness, but have implications for both computational neural modeling and clinical practice, such as in the diagnosis of loss of consciousness in patients with DOC.

Two aspects of the low frequency fluctuations (Biswal et al., 1995; Fox and Raichle, 2007; Zhang and Raichle, 2010) of resting-state fMRI-BOLD signals were suggested as having a role in the neural basis of consciousness: 1) temporal variability (Huang et al., 2014a,b) and 2) brain signal synchronization (Boveroux et al., 2010; Mashour, 2006; Schrouff et al., 2011; Uehara et al., 2013; White and Alkire, 2003). In the first case, our results extend previous observations by showing a global reduction of temporal variability in wide-spread cortical regions measured by SD, and altered spatial (topographical) distribution pattern across midline and lateral cortical regions in anesthesia (measured by SD-Z). This is in line with the increasing evidence that temporal variability of brain activity is a useful attribute of neural systems (Deco et al., 2009, 2011; Faisal et al., 2008; Garrett et al., 2010, 2011, 2013a,b; He, 2011; McIntosh et al., 2010; Shew et al., 2009, 2011; Vakorin et al., 2011). For the second aspect, brain signal synchronization, our results are consistent with recent functional neuroimaging studies that show impaired functional connectivity in the frontoparietal and thalamocortical networks in loss of consciousness, such as during anesthesia (Boveroux et al., 2010; Mashour, 2006; Palanca et al., 2015; Schrouff et al., 2011; White and Alkire, 2003), and in the vegetative state (Demertzi et al., 2014; Kotchoubey et al., 2013; Vanhaudenhuyse et al., 2010).

Theoretically, the scale of the signals (temporal variability) should be independent of the correlation coefficient (signal synchronization). Several studies, however, have revealed a close relationship between the two from both neural modeling (Litwin-Kumar and Doiron, 2012; Yang et al., 2014; Zhigulin et al., 2003) and neuroimaging observations (Abou Elseoud et al., 2014; Di et al., 2013; Huang et al., 2014a,b; Xuan et al., 2012; Yuan et al., 2013). Because of this, there appears to be some ill-defined physiological mechanisms of their relationship that exceeds purely theoretical or mathematical assumptions. Of note, this relationship was carefully examined in a recent fMRI study on schizophrenia by Yang et al. (2014). The authors found abnormal increases of temporal variability in schizophrenia, which can be explained by net increases in local (recurrent self-coupling) and distant (long-range coupling) signal synchronization. Specifically, the authors explored the neurobiological mechanisms using a biophysically based computational model of resting-state fluctuations in multiple parcellated brain regions (Deco et al., 2013). They observed that the temporal variability increased as a function of increasing local and distant signal synchronization. Their result may serve as an initial proof-of-principle of the neural

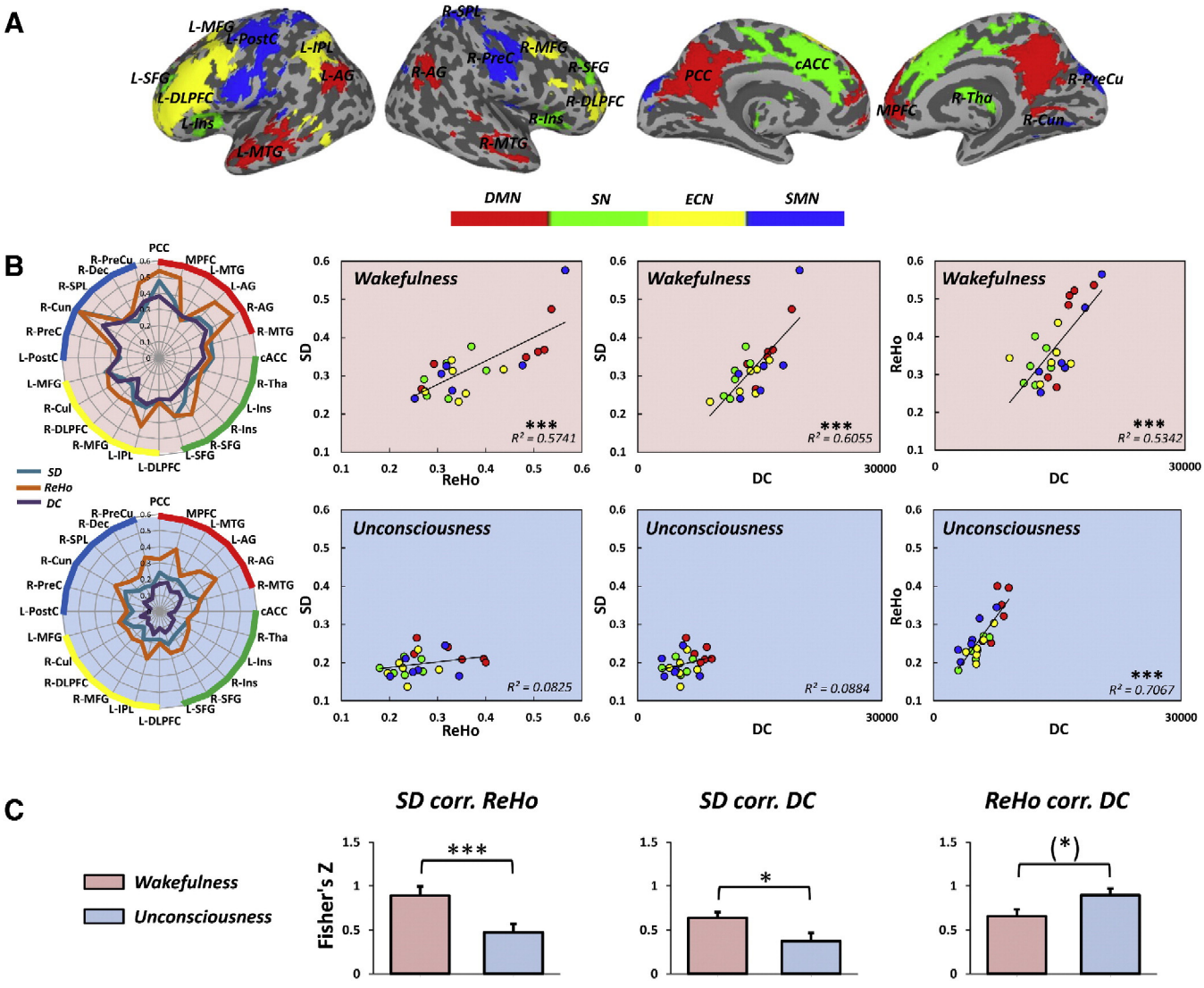

Fig. 2. Decoupled temporal variability and brain signal synchronization in anesthesia. A. Nodes of intrinsic connectivity were defined from four distinct networks: the default mode network (DMN), salience network (SN), executive-control network (ECN) and sensorimotor network (SMN). B. Left: spatial patterns of value distribution of SD, ReHo, and DC (divided by 5000 for visualization purpose) across the 24 nodes for wakefulness (pink background) and unconsciousness (blue background). Right: scatter plots showing the correlation between SD, ReHo and DC during both wakefulness and unconsciousness, respectively. C. Confirmation of node-based correlation analyses. The correlation coefficients (Fisher's Z) of SD ∝ ReHo, SD ∝ DC, and ReHo ∝ DC were first calculated for each subject and then compared between wakefulness and unconsciousness at the group level. ***$p < 0.005$, *$p < 0.05$, (*) marginal significance.

bases of temporal variability, as the model explicitly excludes non-neural signal sources (Yang et al., 2014).

Our results showed that the temporal variability (SD) correlates positively with both local (ReHo) and distant (DC) signal synchronization during wakefulness; the higher the degree of temporal variability, the higher its intra-regional homogeneity and inter-regional functional connectivity. This finding confirms the model prediction by Yang et al. (2014). Interestingly, these correlations were no longer observed in subjects under anesthesia as well as in patients with DOC. These findings, apparently, cannot be explained by their model, because a general reduction of temporal variability and signal synchronization (seen in Fig. 1) does not necessarily lead to a dissociation of the two. However, one important factor that must be taken into account is the "common shared signal" given the known large contribution of global signal in empirical data (Yang et al., 2014). Furthermore, since implementing this common shared global signal component into the model architecture of Yang et al.'s study, their model produced results that 1) best match human patterns of functional connectivity, and 2) build-up a biophysically based linkage between temporal variability and signal synchronization. Therefore, we argue that the decoupling between temporal variability and signal synchronization may indicate a lack of shared signal of global activity, which may be conscious relevant. Nevertheless, future investigations on the origin of the shared signal, as well as other information integration measures, for instance the complexity index (Casali et al., 2013) and transfer entropy (Mäki-Marttunen et al., 2013), are necessary to support such a tentative hypothesis. It is also interesting to better address the validity of our findings by examining more active conscious states during, for instance, basic finger tapping or motor learning (Hardwick et al., 2013).

To distinguish between drug and consciousness-related effects of anesthesia, we included two different subgroups in which anesthesia was induced by drugs with different molecular targets, propofol and sevoflurane (Franks, 2008; Hemmings et al., 2005; Kaisti et al., 2003). We scanned each subjects twice, once awake and once in the anesthetized state, with clear differences between the two states in the SD, ReHo and DC. Despite the fact that propofol and sevoflurane anesthesia

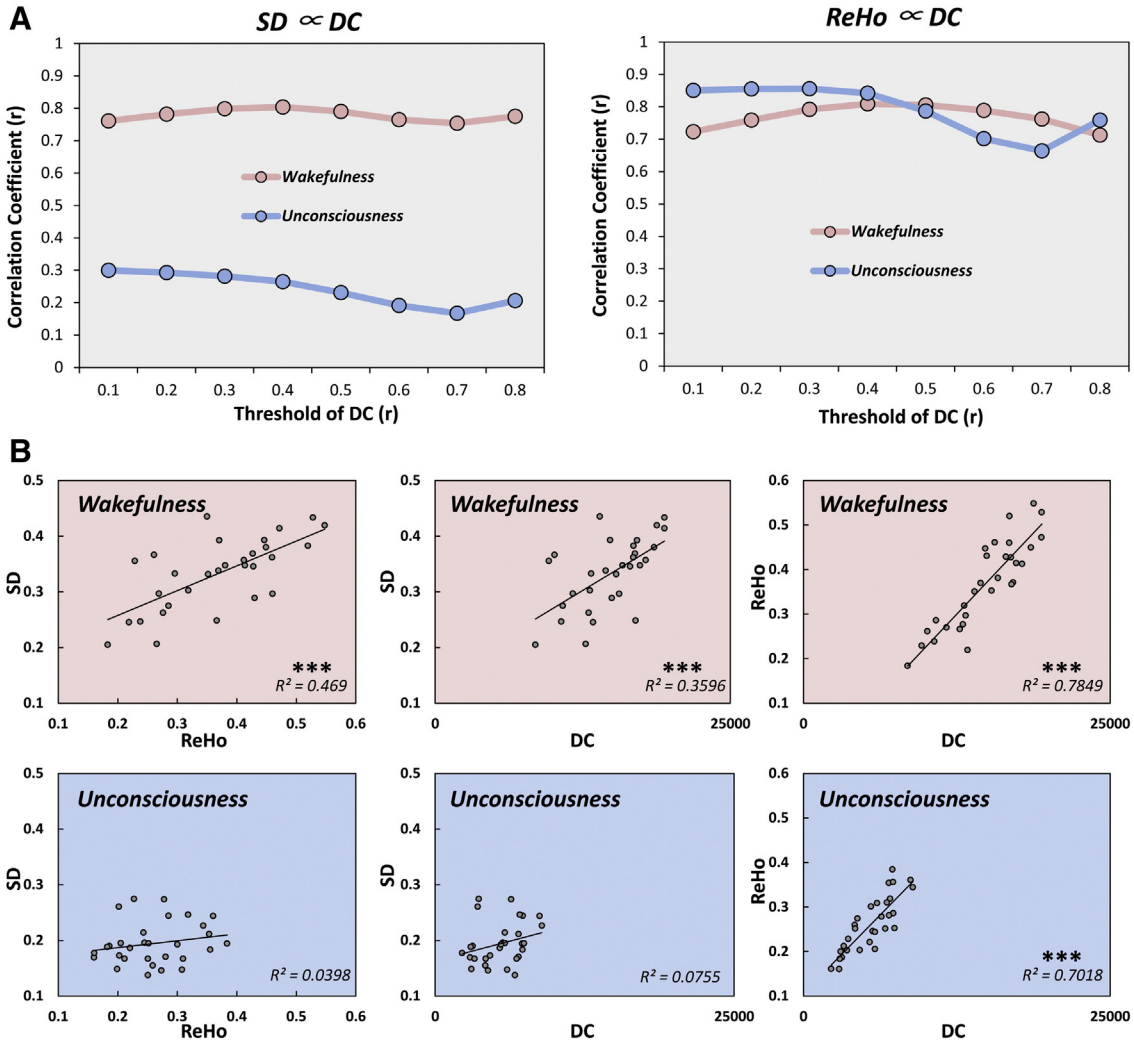

Fig. 3. Group differences (wakefulness vs. unconsciousness) are both robust to the choice of threshold in the DC analysis and nodes definition. A. A range of thresholds ($0.1 \le r \le 0.8$, 0.1 increments) were used to binarize the correlation matrix. Significant differences in SD ∝ DC were seen across all thresholds applied ($p < 0.005$). No significant difference was seen in ReHo ∝ DC for any threshold. B. Ruling out potential bias on nodes definition. All correlation analyses were repeated using another nodes' template (He, 2011). Similar results as those in Fig. 2 were seen. ***$p < 0.005$.

have different physiological effects in terms of regional cerebral blood flow (Kaisti et al., 2002, 2003), regional cerebral glucose metabolism (Jeong et al., 2006), and cerebral perfusion pressure (Marval et al., 2005), our results are not likely due to the drugs themselves. As shown, no interaction effect between conscious state and type of anesthetic agent was found. This was further confirmed using type of anesthetic agent as covariates in standard GLM analyses. We deduce that although the two anesthetic agents have different molecular targets as well as physiological effects, their impact on consciousness may share a common brain network (Franks, 2008; Hemmings et al., 2005; Kaisti et al., 2003). As is known, $GABA_A$ receptors play an important role, or even a causal link, in anesthetic-induced unconsciousness (Franks, 2008). Specifically, the intravenous anesthetics, such as propofol, represent more potent and specific positive modulators of $GABA_A$ receptors by enhancing the gating of the receptors by GABA (Hales and Lambert, 1991; Tomlin et al., 1998) thereby reducing neuronal excitability (Franks, 2006). The volatile anesthetics, on the other hand, such as sevoflurane, enhances $GABA_A$ receptor function (Krasowski and Harrison, 1999) that increases channel opening which enhances inhibition at both synaptic and extrasynaptic receptors (Hemmings et al., 2005). Therefore, it seems both propofol and sevoflurane enhance the function of $GABA_A$ receptors, which is the most abundant fast inhibitory neurotransmitter receptor in the central nerve system. Alternatively, the results could indicate a lack of power in detecting differences between anesthetic agents due to a relatively small sample size. Future studies with larger sample size are needed to provide a final verdict.

More importantly, the decoupling between temporal variability and signal synchronization was reproduced in an independent group of subjects with disorders of consciousness, such as unresponsive wakefulness syndrome and minimally conscious state, using a well-established clinical assessment (Giacino et al., 2004). For this reason, this finding further ruled out the potential drug effects of anesthesia. Taken together, the differences between wakefulness and the anesthetic state observed are likely due to differences in the level of consciousness rather than drug-specific factors.

Finally, an interesting comparison may involve unconscious patients (under anesthesia) and disorders of consciousness (DOC). However, considering that the rs-fMRI datasets of two groups were acquired by different scanners, as well as different scanning parameters, we were unable to make sound inference by comparing them. Future studies with a full factorial design (the degree of consciousness as a factor)

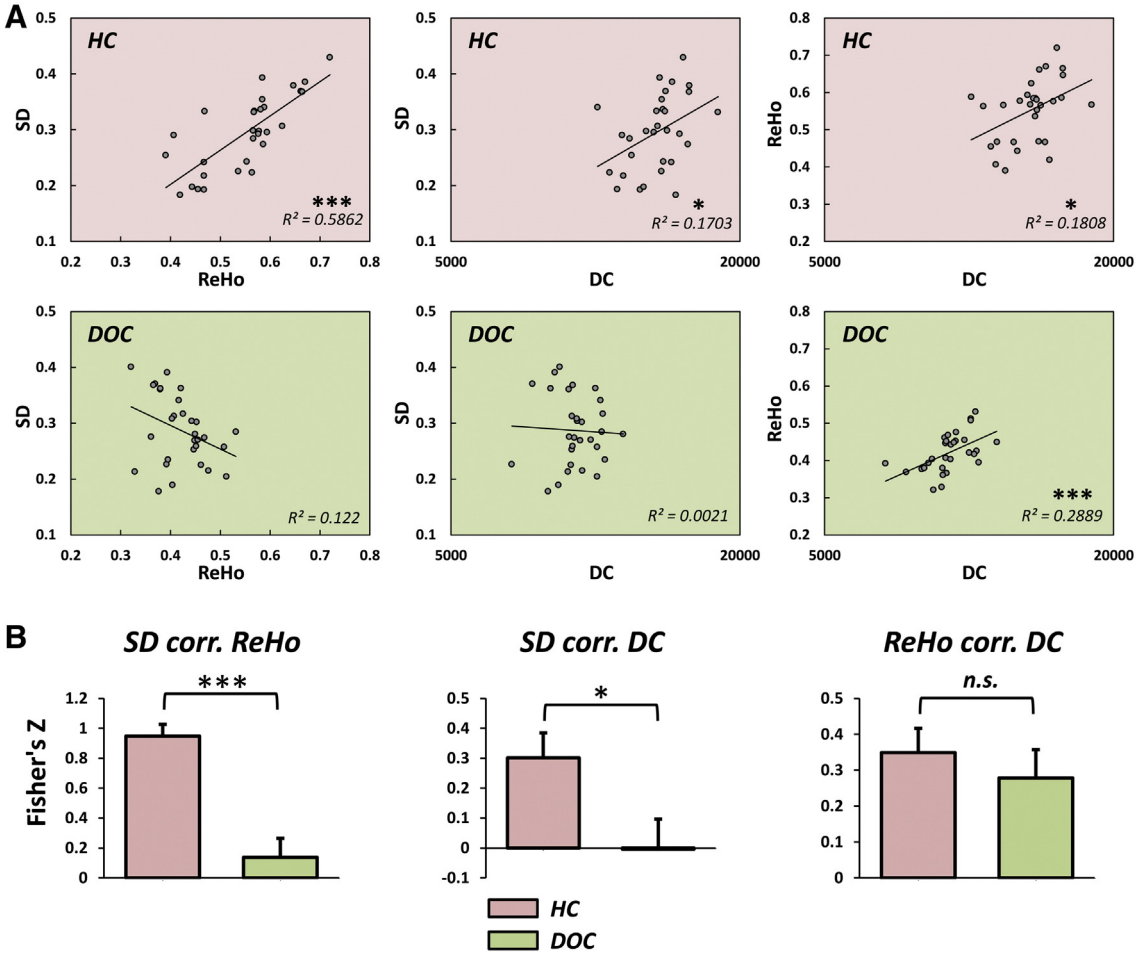

Fig. 4. Decoupled temporal variability and brain signal synchronization in patients with disorders of consciousness (DOC). A. Scatter plots showing the correlation between SD, ReHo and DC for both healthy controls (HC) and DOC patients, respectively. B. Confirmation of node-based correlation analyses. The correlation coefficients (Fisher's Z) of SD ∝ ReHo, SD ∝ DC, and ReHo ∝ DC were first calculated for each subject and then compared between HC and DOC at the group level. ***p < 0.005, *p < 0.05, (n.s.) non-significance.

and larger sample size, including healthy controls, and anesthetized and DOC patients, may potentially provide important insights in terms of the neural correlates of (un)consciousness.

Conclusions

We report, for the first time, a global reduction in the temporal variability, local and distant brain signal synchronization during loss of consciousness in anesthesia. Importantly, we found a decoupling between temporal variability and signal synchronization across various brain regions in anesthesia. Our findings not only extend our current knowledge of the neural correlates of anesthetic-induced unconsciousness, but have implications for both computational neural modeling and clinical practice.

Acknowledgments

This research was supported by the Natural Science Foundation of China (to Jun Zhang, No. 81171020), the EJLB-Michael Smith Foundation (200809EJL-194083-EJL-CECA-179644), the Canada Institute of

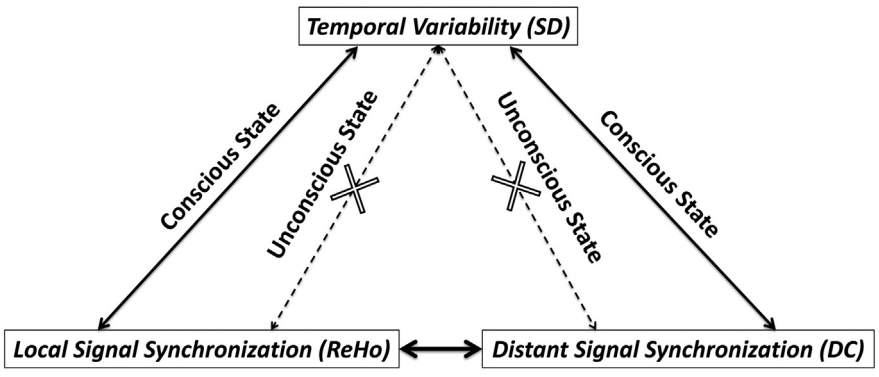

Fig. 5. The temporal variability and signal synchronization are decoupled during unconsciousness.

Health Research (CIHR) (201103MOP-244752-BSB-CECA-179644; 201103CCI-248496-CCI-CECA-179644) (to Georg Northoff). We declare no conflict of interest for all authors.

Appendix A. Supplementary data

Supplementary data to this article can be found online at http://dx.doi.org/10.1016/j.neuroimage.2015.08.062.

References

Abou Elseoud, A., Nissilä, J., Liettu, A., Remes, J., Jokelainen, J., Takala, T., …, Kiviniemi, V., 2014. Altered resting-state activity in seasonal affective disorder. Hum. Brain Mapp. 35 (1), 161–172.

Biswal, B., Yetkin, F.Z., Haughton, V.M., Hyde, J.S., 1995. Functional connectivity in the motor cortex of resting human brain using echo-planar MRI. Magn. Reson. Med. 34, 537–541.

Boveroux, P., Vanhaudenhuyse, A., Bruno, M.-A., Noirhomme, Q., Lauwick, S., Luxen, A., …, Boly, M., 2010. Breakdown of within- and between-network resting state functional magnetic resonance imaging connectivity during propofol-induced loss of consciousness. Anesthesiology 113, 1038–1053.

Buckner, R.L., Sepulcre, J., Talukdar, T., Krienen, F.M., Liu, H., Hedden, T., …, Johnson, K.A., 2009. Cortical hubs revealed by intrinsic functional connectivity: mapping, assessment of stability, and relation to Alzheimer's disease. J. Neurosci. 29 (6), 1860–1873.

Casali, A.G., Gosseries, O., Rosanova, M., Boly, M., Sarasso, S., Casali, K.R., …, Massimini, M., 2013. A theoretically based index of consciousness independent of sensory processing and behavior. Sci. Transl. Med. 5 (198ra105).

Chai, X.J., Castañón, A.N., Ongür, D., Whitfield-Gabrieli, S., 2012. Anticorrelations in resting state networks without global signal regression. NeuroImage 59 (2), 1420–1428.

Chernik, D.A., Gillings, D., Laine, H., Hendler, J., Silver, J.M., Davidson, A.B., …, Siegel, J.L., 1990. Validity and reliability of the Observer's Assessment of Alertness/Sedation Scale: study with intravenous midazolam. J. Clin. Psychopharmacol. 10 (4), 244–251.

Cordes, D., Haughton, V.M., Arfanakis, K., Wendt, G.J., Turski, P.A., Moritz, C.H., …, Meyerand, M.E., 2000. Mapping functionally related regions of brain with functional connectivity MR imaging. Am. J. Neuroradiol. 21, 1636–1644.

Cox, R.W., 1996. AFNI: software for analysis and visualization of functional magnetic resonance neuroimages. Comput. Biomed. Res. Int. J. 29, 162–173.

De Pasquale, F., Della Penna, S., Snyder, A.Z., Marzetti, L., Pizzella, V., Romani, G.L., Corbetta, M., 2012. A cortical core for dynamic integration of functional networks in the resting human brain. Neuron 74 (4), 753–764.

Deco, G., Jirsa, V.K., 2012. Ongoing cortical activity at rest: criticality, multistability, and ghost attractors. J. Neurosci. 32, 3366–3375.

Deco, G., Jirsa, V., McIntosh, A.R., Sporns, O., Kötter, R., 2009. Key role of coupling, delay, and noise in resting brain fluctuations. Proc. Natl. Acad. Sci. U. S. A. 106, 10302–10307.

Deco, G., Jirsa, V.K., McIntosh, A.R., 2011. Emerging concepts for the dynamical organization of resting-state activity in the brain. Nat. Rev. Neurosci. 12, 43–56.

Deco, G., Ponce-Alvarez, A., Mantini, D., Romani, G.L., Hagmann, P., Corbetta, M., 2013. Resting-state functional connectivity emerges from structurally and dynamically shaped slow linear fluctuations. J. Neurosci. 33 (27), 11239–11252.

Demertzi, A., Gómez, F., Crone, J.S., Vanhaudenhuyse, A., Tshibanda, L., Noirhomme, Q., …, Soddu, A., 2014. Multiple fMRI system-level baseline connectivity is disrupted in patients with consciousness alterations. Cortex 52, 35–46.

Di Martino, A., Zuo, X.-N., Kelly, C., Grzadzinski, R., Mennes, M., Schvarcz, A., …, Milham, M.P., 2013. Shared and distinct intrinsic functional network centrality in autism and attention-deficit/hyperactivity disorder. Biol. Psychiatry 74 (8), 623–632.

Di, X., Kim, E.H., Huang, C.-C., Tsai, S.-J., Lin, C.-P., Biswal, B.B., 2013. The influence of the amplitude of low-frequency fluctuations on resting-state functional connectivity. Front. Hum. Neurosci. 7 (April), 118.

Eckert, M.A., Menon, V., Walczak, A., Ahlstrom, J., Denslow, S., Horwitz, A., Dubno, J.R., 2009. At the heart of the ventral attention system: the right anterior insula. Hum. Brain Mapp. 30 (8), 2530–2541.

Faisal, A.A., Selen, L.P.J., Wolpert, D.M., 2008. Noise in the nervous system. Nat. Rev. Neurosci. 9, 292–303.

Fox, M.D., Raichle, M.E., 2007. Spontaneous fluctuations in brain activity observed with functional magnetic resonance imaging. Nat. Rev. Neurosci. 8 (9), 700–711.

Fox, M.D., Snyder, A.Z., Vincent, J.L., Corbetta, M., Van Essen, D.C., Raichle, M.E., 2005. The human brain is intrinsically organized into dynamic, anticorrelated functional networks. Proc. Natl. Acad. Sci. U. S. A. 102 (27), 9673–9678.

Franks, N.P., 2006. Molecular targets underlying general anaesthesia. Br. J. Pharmacol. 147, S72–S81.

Franks, N.P., 2008. General anaesthesia: from molecular targets to neuronal pathways of sleep and arousal. Nat. Rev. Neurosci. 9 (5), 370–386.

Garrett, D.D., Kovacevic, N., McIntosh, A.R., Grady, C.L., 2010. Blood oxygen level-dependent signal variability is more than just noise. J. Neurosci. 30, 4914–4921.

Garrett, D.D., Kovacevic, N., McIntosh, A.R., Grady, C.L., 2011. The importance of being variable. J. Neurosci. 31 (12), 4496–4503.

Garrett, D.D., Kovacevic, N., McIntosh, A.R., Grady, C.L., 2013a. The modulation of BOLD variability between cognitive states varies by age and processing speed. Cereb. Cortex 23 (3), 684–693.

Garrett, D.D., McIntosh, A.R., Grady, C.L., 2013b. Brain signal variability is parametrically modifiable. Cereb. Cortex 5, 1–10.

Garrett, D.D., Samanez-Larkin, G.R., MacDonald, S.W., Lindenberger, U., McIntosh, A.R., Grady, C.L., 2013c. Moment-to-moment brain signal variability: a next frontier in human brain mapping? Neurosci. Biobehav. Rev. 37 (4), 610–624.

Giacino, J.T., Kalmar, K., Whyte, J., 2004. The JFK Coma Recovery Scale — Revised: measurement characteristics and diagnostic utility. Arch. Phys. Med. Rehabil. 85 (12), 2020–2029.

Greicius, M.D., Krasnow, B., Reiss, A.L., Menon, V., 2003. Functional connectivity in the resting brain: a network analysis of the default mode hypothesis. Proc. Natl. Acad. Sci. U. S. A. 100 (1), 253–258.

Greicius, M.D., Srivastava, G., Reiss, A.L., Menon, V., 2004. Default-mode network activity distinguishes Alzheimer's disease from healthy aging: evidence from functional MRI. Proc. Natl. Acad. Sci. U. S. A. 101 (13), 4637–4642.

Hales, T.G., Lambert, J.J., 1991. The actions of propofol on inhibitory amino acid receptors of bovine adrenomedullary chromaffin cells and rodent central neurones. Br. J. Pharmacol. 104, 619–628.

Hardwick, R.M., Rottschy, C., Miall, R.C., Eickhoff, S.B., 2013. A quantitative meta-analysis and review of motor learning in the human brain. NeuroImage 67, 283–297.

He, B.J., 2011. Scale-free properties of the functional magnetic resonance imaging signal during rest and task. J. Neurosci. 31 (39), 13786–13795.

He, B.J., 2013. Spontaneous and task-evoked brain activity negatively interact. J. Neurosci. 33 (11), 4672–4682.

He, B.J., Zempel, J.M., Snyder, A.Z., Raichle, M.E., 2010. The temporal structures and functional significance of scale-free brain activity. Neuron 66 (3), 353–369.

Heine, L., Soddu, A., Gómez, F., Vanhaudenhuyse, A., Tshibanda, L., Thonnard, M., …, Demertzi, A., 2012. Resting state networks and consciousness: alterations of multiple resting state network connectivity in physiological, pharmacological, and pathological consciousness States. Front. Psychol. 3 (August), 295.

Hemmings, H.C., Akabas, M.H., Goldstein, P.A., Trudell, J.R., Orser, B.A., Harrison, N.L., 2005. Emerging molecular mechanisms of general anesthetic action. Trends Pharmacol. Sci. 26 (10), 503–510.

Huang, Z., Dai, R., Wu, X., Yang, Z., Liu, D., Hu, J., …, Northoff, G., 2014a. The self and its resting state in consciousness: an investigation of the vegetative state. Hum. Brain Mapp. 35 (5), 1997–2008.

Huang, Z., Wang, Z., Zhang, J., Dai, R., Wu, J., Li, Y., …, Northoff, G., 2014b. Altered temporal variance and neural synchronization of spontaneous brain activity in anesthesia. Hum. Brain Mapp. 35 (11), 5368–5378.

Jeong, Y.B., Kim, J.S., Jeong, S.M., Park, J.W., Choi, I.C., 2006. Comparison of the effects of sevoflurane and propofol anaesthesia on regional cerebral glucose metabolism in humans using positron emission tomography. J. Int. Med. Res. 34 (4), 374–384.

Kaisti, K.K., Metsähonkala, L., Teräs, M., Oikonen, V., Aalto, S., Jääskeläinen, S., …, Scheinin, H., 2002. Effects of surgical levels of propofol and sevoflurane anesthesia on cerebral blood flow in healthy subjects studied with positron emission tomography. Anesthesiology 96 (6), 1358–1370.

Kaisti, K.K., Långsjö, J.W., Aalto, S., Oikonen, V., Sipilä, H., Teräs, M., …, Scheinin, H., 2003. Effects of sevoflurane, propofol, and adjunct nitrous oxide on regional cerebral blood flow, oxygen consumption, and blood volume in humans. Anesthesiology 99, 603–613.

Katoh, T., Ikeda, K., 1998. The effects of fentanyl on sevoflurane requirements for loss of consciousness and skin incision. Anesthesiology 88, 18–24.

Kotchoubey, B., Merz, S., Lang, S., Markl, A., Müller, F., Yu, T., Schwarzbauer, C., 2013. Global functional connectivity reveals highly significant differences between the vegetative and the minimally conscious state. J. Neurol. 260 (4), 975–983.

Krasowski, M.D., Harrison, N.L., 1999. General anaesthetic actions on ligand-gated ion channels. Cell. Mol. Life Sci. 55, 1278–1303.

Laird, A.R., Eickhoff, S.B., Li, K., Robin, D.A., Glahn, D.C., Fox, P.T., 2009. Investigating the functional heterogeneity of the default mode network using coordinate-based meta-analytic modeling. J. Neurosci. 29 (46), 14496–14505.

Litwin-Kumar, A., Doiron, B., 2012. Slow dynamics and high variability in balanced cortical networks with clustered connections. Nat. Neurosci. 15 (11), 1498–1505.

Liu, S.H., Wei, W., Ding, G.N., Ke, J.D., Hong, F.X., Tian, M., 2009. Relationship between depth of anesthesia and effect-site concentration of propofol during induction with the target-controlled infusion technique in elderly patients. Chin. Med. J. 122 (8), 935–940.

Mäki-Marttunen, V., Diez, I., Cortes, J.M., Chialvo, D.R., Villarreal, M., 2013. Disruption of transfer entropy and inter-hemispheric brain functional connectivity in patients with disorder of consciousness. Front. Neuroinform. 7 (November), 24.

Marval, P.D., Perrin, M.E., Hancock, S.M., Mahajan, R.P., 2005. The effects of propofol or sevoflurane on the estimated cerebral perfusion pressure and zero flow pressure. Anesth. Analg. 100 (3), 835–840.

Mashour, G.A., 2006. Integrating the science of consciousness and anesthesia. Anesth. Analg. 103, 975–982.

McIntosh, A.R., Kovacevic, N., Lippe, S., Garrett, D., Grady, C., Jirsa, V., 2010. The development of a noisy brain. Arch. Ital. Biol. 148, 323–337.

Palanca, B.J., Mitra, A., Larson-Prior, L., Snyder, A.Z., Avidan, M.S., Raichle, M.E., 2015. Resting-state functional magnetic resonance imaging correlates of sevoflurane-induced unconsciousness. Anesthesiology (Epub ahead of print).

Power, J.D., Barnes, K.A., Snyder, A.Z., Schlaggar, B.L., Petersen, S.E., 2012. Spurious but systematic correlations in functional connectivity MRI networks arise from subject motion. NeuroImage 59, 2142–2154.

Preston, A.R., Thomason, M.E., Ochsner, K.N., Cooper, J.C., Glover, G.H., 2004. Comparison of spiral-in/out and spiral-out BOLD fMRI at 1.5 and 3 T. NeuroImage 21 (1), 291–301.

Quan, X., Yi, J., Ye, T.H., Tian, S.Y., Zou, L., Yu, X.R., Huang, Y.G., 2013. Propofol and memory: a study using a process dissociation procedure and functional magnetic resonance imaging. Anaesthesia 68 (4), 391–399.

Raichle, M.E., MacLeod, A.M., Snyder, A.Z., Powers, W.J., Gusnard, D.A., Shulman, G.L., 2001. A default mode of brain function. Proc. Natl. Acad. Sci. U. S. A. 98 (2), 676–682.

Sadaghiani, S., Hesselmann, G., Kleinschmidt, A., 2009. Distributed and antagonistic contributions of ongoing activity fluctuations to auditory stimulus detection. J. Neurosci. 29, 13410–13417.
Sadaghiani, S., Scheeringa, R., Lehongre, K., Morillon, B., Giraud, A.-L., Kleinschmidt, A., 2010. Intrinsic connectivity networks, alpha oscillations, and tonic alertness: a simultaneous electroencephalography/functional magnetic resonance imaging study. J. Neurosci. 30 (30), 10243–10250.
Schrouff, J., Perlbarg, V., Boly, M., Marrelec, G., Boveroux, P., Vanhaudenhuyse, A., ... Benali, H., 2011. Brain functional integration decreases during propofol-induced loss of consciousness. NeuroImage 57 (1), 198–205.
Seeley, W.W., Menon, V., Schatzberg, A.F., Keller, J., Glover, G.H., Kenna, H., …, Greicius, M.D., 2007. Dissociable intrinsic connectivity networks for salience processing and executive control. J. Neurosci. 27 (9), 2349–2356.
Shew, W.L., Yang, H., Petermann, T., Roy, R., Plenz, D., 2009. Neuronal avalanches imply maximum dynamic range in cortical networks at criticality. J. Neurosci. 29, 15595–15600.
Shew, W.L., Yang, H., Yu, S., Roy, R., Plenz, D., 2011. Information capacity and transmission are maximized in balanced cortical networks with neuronal avalanches. J. Neurosci. 31, 55–63.
Talairach, J., Tournoux, P., 1988. Co-planar Stereotaxic Atlas of the Human Brain. New York: G. Thieme; Thieme Medical Publishers, Stuttgart.
Tomlin, S.L., Jenkins, A., Lieb, W.R., Franks, N.P., 1998. Stereoselective effects of etomidate optical isomers on gamma-aminobutyric acid type A receptors and animals. Anesthesiology 88, 708–717.
Uehara, T., Yamasaki, T., Okamoto, T., Koike, T., Kan, S., Miyauchi, S., …, Tobimatsu, S., 2013. Efficiency of a "small-world" brain network depends on consciousness level: a resting-state fMRI study. Cereb. Cortex http://dx.doi.org/10.1093/cercor/bht004.
Vakorin, V.A., Lippé, S., McIntosh, A.R., 2011. Variability of brain signals processed locally transforms into higher connectivity with brain development. J. Neurosci. 31, 6405–6413.
Van Dijk, K.R.A., Sabuncu, M.R., Buckner, R.L., 2012. The influence of head motion on intrinsic functional connectivity MRI. NeuroImage 59, 431–438.
Vanhaudenhuyse, A., Noirhomme, Q., Tshibanda, L.J.-F., Bruno, M.-A., Boveroux, P., Schnakers, C., …, Boly, M., 2010. Default network connectivity reflects the level of consciousness in non-communicative brain-damaged patients. Brain 133 (Pt 1), 161–171.
White, N.S., Alkire, M.T., 2003. Impaired thalamocortical connectivity in humans during general-anesthetic-induced unconsciousness. NeuroImage 19 (2), 402–411.
Wong, K.F., Wang, X.J., 2006. A recurrent network mechanism of time integration in perceptual decisions. J. Neurosci. 26 (4), 1314–1328.
Xu, Z., Liu, F., Yue, Y., Ye, T., Zhang, B., Zuo, M., …, Che, X., 2009. C50 for propofol–remifentanil target-controlled infusion and bispectral index at loss of consciousness and response to painful stimulus in Chinese patients: a multicenter clinical trial. Anesth. Analg. 108, 478–483.
Xuan, Y., Meng, C., Yang, Y., Zhu, C., Wang, L., Yan, Q., …, Yu, C., 2012. Resting-state brain activity in adult males who stutter. PLoS One 7 (1), e30570.
Yang, G.J., Murray, J.D., Repovs, G., Cole, M.W., Savic, A., Glasser, M.F., …, Anticevic, A., 2014. Altered global brain signal in schizophrenia. Proc. Natl. Acad. Sci. U. S. A. 111 (20), 7438–7443.
Yuan, R., Di, X., Kim, E.H., Barik, S., Rypma, B., Biswal, B.B., 2013. Regional homogeneity of resting-state fMRI contributes to both neurovascular and task activation variations. Magn. Reson. Imaging 31 (9), 1492–1500.
Zang, Y., Jiang, T., Lu, Y., He, Y., Tian, L., 2004. Regional homogeneity approach to fMRI data analysis. NeuroImage 22 (1), 394–400.
Zang, Y., He, Y., Zhu, C.-Z., Cao, Q.-J., Sui, M.-Q., Liang, M., …, Wang, Y.-F., 2007. Altered baseline brain activity in children with ADHD revealed by resting-state functional MRI. Brain Dev 29 (2), 83–91.
Zhang, D., Raichle, M.E., 2010. Disease and the brain's dark energy. Nat. Rev. Neurol. 6, 15–28.
Zhang, H., Wang, W., Gao, W., Ge, Y., Zhang, J., Wu, S., Xu, L., 2009. Effect of propofol on the levels of neurotransmitters in normal human brain: a magnetic resonance spectroscopy study. Neurosci. Lett. 467 (3), 247–251.
Zhigulin, V., Rabinovich, M., Huerta, R., Abarbanel, H., 2003. Robustness and enhancement of neural synchronization by activity-dependent coupling. Phys. Rev. E 67 (2), 021901.
Zuo, X.-N., Di Martino, A., Kelly, C., Shehzad, Z.E., Gee, D.G., Klein, D.F., …, Milham, M.P., 2010. The oscillating brain: complex and reliable. NeuroImage 49 (2), 1432–1445.
Zuo, X.-N., Ehmke, R., Mennes, M., Imperati, D., Castellanos, F.X., Sporns, O., Milham, M.P., 2012. Network centrality in the human functional connectome. Cereb. Cortex 22 (8), 1862–1875.
Zuo, X.-N., Xu, T., Jiang, L., Yang, Z., Cao, X.-Y., He, Y., …, Milham, M.P., 2013. Toward reliable characterization of functional homogeneity in the human brain: preprocessing, scan duration, imaging resolution and computational space. NeuroImage 65, 374–386.